$K\alpha_{1,2}$ and $K\beta_{1,3}$ x-ray emission lines of the $3d$ transition metals

G. Hölzer,[1] M. Fritsch,[1,2] M. Deutsch,[2] J. Härtwig,[3] and E. Förster[1]
[1]*X-ray Optics Group, Institute of Optics and Quantum Electronics, Friedrich-Schiller-University Jena, Max-Wien-Platz 1, D-07743 Jena, Germany*
[2]*Physics Department, Bar-Ilan University, Ramat-Gan 52900, Israel*
[3]*European Synchrotron Radiation Facility, Boîte Postale 220, F-38043 Grenoble, France*
(Received 14 May 1997)

The $K\alpha_{1,2}$ and $K\beta_{1,3}$ emission spectra of the $3d$ transition metals Cr, Mn, Fe, Co, Ni, and Cu were measured, employing a single-crystal diffractometer optimized for minimal instrumental broadening. The high-accuracy diffractometer, and the interferometrically calibrated silicon crystal employed ensure *absolute* wavelengths in the metric scale to a sub-part-per-million accuracy. An accurate analytic representation of each line, obtained by a fit to a minimal set of Lorentzians, is presented. The absolute energies, linewidths, and indices of asymmetry, derived from the data, agree well with previous measurements. So do also the intensity ratios $K\alpha_2/K\alpha_1$ and $K\beta_{1,3}/K\alpha_{1,2}$, which are, however, slightly, but consistently, higher than previous values. Possible origins for the observed Z-dependent trends are discussed. [S1050-2947(97)03012-6]

PACS number(s): 32.30.Rj, 32.80.Hd, 31.30.Jv

I. INTRODUCTION

Simultaneous multielectronic transitions within the atom play an important role in determining the structure in and the intensities of x-ray emission spectra. This is particularly true in the case of the $3d$ transition metals, whose asymmetric line shapes were attributed as early as 1928 to contributions from two-electron transitions [1]. Several other mechanisms such as conduction-band collective excitations [2], exchange [3], and final-state interactions [4] were also suggested as equally probable alternatives. In spite of an extended and extensive research effort over several decades [5] no final agreement on the physics underlying these line shapes emerged. Very recently, combining precision line-shape measurements and *ab initio* relativistic Dirac-Fock calculations, we were able to show that the line shapes of the Cu $K\alpha$ and $K\beta$ emission lines can be fully accounted for by contributions from $\underline{3d}$-spectator transitions only, in addition to the diagram ones [5] (in the following, underlining denotes hole states). This conclusion was strongly supported by the considerably improved agreement with theory of the L and M level widths and fluorescence yields, which now could be derived from the diagram contributions only, after stripping off from the measured lines those due to the spectator transitions [6]. High-resolution measurements of these spectra photoexcited at energies near the K edge show clearly the first appearance of the asymmetric features at an excitation energy coinciding with the calculated threshold for creation of a $\underline{1s3d}$ two-hole configuration, which is the initial state of the $\underline{3d}$-spectator transitions [7]. While these results support very convincingly a two-electron excitation origin for the line-shape asymmetry in Cu, it is clear that for this interpretation to be conclusive, neighboring $3d$ elements must be shown to have a similar behavior. To our knowledge, suitable high-resolution spectra for such a study are, however, not available at present, nor has there been any in-depth study, such as that discussed above for Cu, for any other element. We have, therefore, undertaken measurements of suitable spectra for 5 other elements, namely, Cr, Mn, Co, Fe, and Ni as a first part of a study similar to that of Cu. The results of these measurements are presented in this paper. Their strength lies in being the only set of $K\alpha$ and $K\beta$ emission lines for (almost) all of the transition metals, which were measured on the same instrument under highly optimized conditions and on an absolute energy scale of sub-parts-per-million (ppm) accuracy. The optimization, based on a detailed study of the instrumental effects involved [8], ensures a minimization of the distortions introduced by them, and allows the removal of any remaining distortion by numerical methods. These procedures are crucial for obtaining reliable and accurate spectra, as found in the Cu study [5]. Precise knowledge of the line shapes and their accurate representation by analytical forms such as the sums of Lorentzians employed here and elsewhere [5,9] are also important for applications in high-precision x-ray diffractometry. These are, for example, stress and grain size determination by line profile analysis of polycrystalline materials and high-precision crystal lattice parameter measurements [10]. Our results should prove, therefore, useful in these fields as well.

This paper presents and discusses the measured spectra. Accurate analytic representations of the line shapes are given, in terms of sums of Lorentzians fitted to the data, for the applications discussed above. Characteristic quantities such as positions of line maxima, linewidths, indices of asymmetry, etc. are determined and compared with the numerous separate measurements of individual lines available in the literature. Finally, the intensity ratios $K\alpha_2/K\alpha_1$ and $K\beta_{1,3}/K\alpha_{1,2}$ are derived from the fits and critically compared with previous measurements.

II. EXPERIMENT

A. Measurement setup

The measurements were performed using a high-precision single-crystal spectrometer [11] in the classical Bragg geometry. The instrument is of a high mechanical stability. Its

TABLE I. Measurement parameters for the line-shape determination. The angular widths $\Delta\theta_s$, which correspond to the width of the spectral line, and $\Delta\theta_d$, which is the ''spectrometer window,'' as well as their ratio, are also listed. A positive asymmetry for a given monochromator crystal reflection indicates grazing incidence relative to the crystal surface.

Element	Line	Reflection	U [kV] / I [mA]	Bragg angle (deg)	Asymmetry angle (deg)	Slit width hor. (mm)	$\Delta\theta_s$ (s)	$\Delta\theta_d$ (s)	$\Delta\theta_s/\Delta\theta_d$
Cr	$K\alpha_1$	331	40 / 30	66.76	22.0	0.04	176.5	21.2	8.3
	$K\beta$	331		56.79	22.0		131.4		6.2
		422		70.11	19.5		239.7		11.3
Mn	$K\alpha_1$	422	30 / 20	71.43	19.5	0.04	247.7	21.2	11.7
	$K\beta$	422		59.49	19.5		160.7		7.6
Fe	$K\alpha_1$	333	25 / 32	67.85	0	0.04	200.2	21.2	9.5
	$K\beta$	333		57.18	0		156.8		7.4
		531		73.10	−28.6		332.8		15.7
Co	$K\alpha_1$	531	30 / 35	77.00	−28.6	0.04	291.4	21.2	13.7
	$K\beta$	531		61.99	−28.6		223.0		10.5
		620		70.69	43.1		338.6		16.0
Ni	$K\alpha_1$	620	30 / 35	74.48	43.1	0.03	214.5	15.9	13.5
	$K\beta$	620		60.87	43.1		245.0		15.4
		444		73.11	0		449.6		28.3
Cu	$K\alpha_1$	444	40 / 32	79.30	0	0.03	328.3	15.9	20.7
		333		47.48	0		65.1		4.1
	$K\beta$	444		62.63	0		265.8		16.7
		553	40 / 30	79.91	12.3	0.10	770.6		48.5

mean total angle dividing accuracy in the absolute position over the full angular interval of 2π is 0.12 arcsec and its minimal angular step is 0.06 arcsec. A silicon crystal with the surface orientation (111) of WASO9 type (obtained from Wacker Chemitronic, Burghausen) was used to measure the emission lines for most of the $3d$ transition metals. Its lattice parameter a was determined in the metrical system by means of combined x-ray and optical interferometry [12] with an accuracy of [13] $\Delta a/a = 9.6\times10^{-8}$ and allows the determination of the emission line peak positions on an absolute energy scale with high accuracy.

The incident beam collimator consists of a 390 mm long tube with crossed slits at both ends, directly attached to the x-ray tube. For all measurements the vertical slit heights were fixed at 0.42 mm while the horizontal widths varied as required. The total air-path length of the radiation from the x-ray tube to the detector is 800 mm. The x-ray generator is a highly stabilized ID3000 from Seifert GmbH&Co KG. The stability was tested in a 60-h run. No measurable drift of the x-ray intensity was observed. Stability against temperature variation was ensured by locating the spectrometer and the x-ray generator in separate basement rooms. The x-ray tube excitation conditions are given in Table I and are always operated with the standards used in x-ray tube applications, with excitation energies much higher than the corresponding K-edge energy of the anode material. Line-shape variations with exciting energy are not expected in this region [7]. Temperature and air pressure were measured at each point and the intensity measured was corrected to correspond to standard conditions ($T = 293.15$ K, $p = 101.325$ kPa). The absorption in air and Be was calculated using absorption coefficients from Henke *et al.* [14] for the wavelength at the maximum of each spectrum.

B. Resolution and instrument function

A major problem for any line-shape measurement, including those using single- and double-crystal spectrometry, is the evaluation of the ''true'' emission line from the measured and instrumentally distorted profile. Preferably, the influence of the instrumental function should be minimized already in the measurement process itself by an optimal selection of the experimental setup. This has been done in our experiments on the basis of computer simulations of the spectrometer window function for our case [8]. The influence of the collimator geometry, the crystal reflection properties (as given by the dynamical theory of x-ray diffraction), the tube arrangement and the absorption of the radiation in the anode, air and windows were taken into account. If the instrumental window is much narrower (ideally a δ function) than the spectral linewidth, the measured line profile corresponds to the ''true'' emission line profile to a very good approximation. In this case, the measured data can be corrected numerically for any small remaining distortion due to the instrumental function. It should be noted that in general the measured emission line is not a convolution of the ''true'' emission line and the instrumental window. Only under special conditions, selected according to our computer simulations and used in the measurements, can the measured data be approximated well by such a convolution, and the evaluation of the ''true'' emission line profile can be done by a deconvolution of the measured spectrum by the instrumental function [8].

The ratio $\Delta\theta_s/\Delta\theta_d$ of the spectral linewidth $\Delta\theta_s$ to the beam divergence $\Delta\theta_d$ (spectrometer window) can be used as a measure of the achievable resolution. Note, however, that in general, the spectrometer window function includes the effects of both the beam divergence (collimator divergence function) and the crystal's angular acceptance function. Only when the latter is of negligible width relative to the beam divergence, as is the case here, can the window function be approximated well by the beam divergence $\Delta\theta_d$. The value of $\Delta\theta_s$ depends, among other parameters, strongly on the Bragg reflection used. Since the calibrated silicon crystal has the surface orientation (111), the number of available reflections and especially of those providing a good resolution (large Bragg angles) is very limited. $\Delta\theta_s$ and $\Delta\theta_d$ are given in Table I. For a single-crystal spectrometer the (horizontal) slit widths of the collimator are the crucial factors for the width of the instrumental function. They should be as small as possible while still allowing a sufficiently high count rate for good statistics. The widths used for the line-shape measurements were between 0.03 and 0.05 mm. The measured emission lines were registered with about 1000 steps and measuring times between 100 and 200 s at each point. The total counts collected at a single point at the peak varied between 20 000 and 50 000 counts for $K\alpha$ and 2000 and 6000 for $K\beta$. In the measurements of the absolute peak position, discussed below, it was found advantageous to choose these three parameters (steps, time, and total counts) differently.

Most of the $K\beta$ spectra used for the determination of the emission line shape were measured with two different reflections. One was the same reflection used for measuring of the $K\alpha$ doublet. This was not necessarily the one with the highest resolution, but it guaranteed the highest possible compatibility in the measuring conditions for the determination of the $K\beta_{1,3}/K\alpha_{1,2}$ intensity ratio. The second reflection was optimized for high resolution (see Table I). The experimental conditions were invariably set so that the effect of the instrumental window function could be removed by deconvoluting the measured data by the simulated instrumental function [8]. The measured data were also corrected for the relative change in absorption and in the integrated reflectivity over the wavelength range. No additional smoothing was applied to the data.

The peak positions of the lines were determined on an absolute energy-wavelength scale in separate measurements according to the Bond method [15]. This method, developed for the diffractometric measurement of lattice parameters of nearly perfect crystals with high accuracy when the energy of the line is known accurately, may be used in reverse to determine the absolute energy, when the lattice parameter of the crystal is known accurately [16]. The optimum experimental conditions in that case are similar to those for the line-shape determination (a large ratio $\Delta\theta_s/\Delta\theta_d$, and, in particular, a large Bragg angle), but the strategy for the measurement and the data analysis is different. The basic task is to determine the kinematical Bragg angle of the selected crystal reflection from the measured intensity distribution. The basics of the measurement strategy are described in detail in [8,17]. 20–25 points were measured spanning the part of the peak whose intensity I is $\geqslant 80\%$ of the maximum. The slit width is selected so that about 50 000 counts (Cr, Mn $K\alpha$, Co $K\beta$, Fe $K\alpha$) and about 100 000 counts (Co $K\alpha$, Ni, Cu) were collected at the maximum. For some lines a smaller number of counts was used (for Mn $K\beta$ 25 000 counts and for Fe $K\beta$ 11 000 counts). Rather than a single scan with a long measuring time at each point a repeated scan technique was used, with a shorter time at each point and each scan repeated from 20 to 40 times. With this strategy obvious runaway scans are easily excluded and the long-time stability of the generator is not stressed to its maximum extent. The energy of the line is determined from the angular position of the intensity profile's peak, through Bragg's law. This profile is, under optimized conditions, a convolution of a wide instrumental function (containing basically the wide collimator function and especially the wide spectral line itself) and the narrow dynamical reflection curve. The peak position determination is done best by calculating that intensity distribution [8] using the emission line shape (with its exact absolute energy scale still unknown) represented by the Lorentzian fit (see Sec. III B), and fitting it to the measured intensity distribution, varying only its height and position [17]. Thus, to determine the line position with high accuracy, its shape must be known. Finally the determination of the peak position of the emission line in the absolute energy or wavelength scale, i.e., in eV or nm, respectively, is possible using the Bragg equation, the kinematical Bragg angle, and the lattice parameter of the calibrated silicon crystal. The conversion factor from the wavelength to the energy scale is [18] $8.065541(3)\times 10^5(\text{m eV})^{-1}$. A careful analysis of the accuracy of Bragg angle measurements and of the possible aberrations was given in [19]. Since no deconvolution of the measured spectrum by the instrumental function is carried out in the case of the line position determination, the horizontal slit width could be chosen larger than for the line-shape determination in order to get more intensity. A width of $\sim$ 0.1 mm was selected.

III. RESULTS AND DISCUSSION

A. Introduction

In this section we present the measured $K\alpha$ and $K\beta$ emission spectra of Cr, Mn, Fe, Co, Ni, and Cu. The ''true'' emission line profiles were determined through deconvolution by the simulated instrumental function of the single-crystal spectrometer [8], as detailed above. Each line was fitted by a sum of Lorentzians to get an accurate analytic, though phenomenological, representation of the line shape for use in x-ray line profile analysis and other applications. The line parameters, i.e., full width at half maximum (FWHM), index of asymmetry, and integrated intensity were determined and are critically compared below with previous measurements, where available. Finally, the $K\alpha_2/K\alpha_1$ and $K\beta_{1,3}/K\alpha_{1,2}$ intensity ratios are calculated and discussed.

B. Lorentzian fit

An accurate analytical representation of the emission line shape is essential for a large number of practical applications of x rays (e.g., grain size and strain determination from single-crystal diffraction line profile analysis of polycrystalline samples [10], structure refinement from powder diffraction patterns, etc.). In both the classical and quantum theory

the natural shape of an emission line in the frequency or energy scale is a Lorentzian [20]. This is observed in practice for a large number of $K\alpha$ emission lines. They are highly symmetric and the $K\alpha$ doublet structure can be represented accurately by a superposition of two Lorentzians, one each for the $K\alpha_1$ and the $K\alpha_2$ lines [21].

By contrast, it is well known that the experimentally observed $K\alpha$ and $K\beta$ emission lines of the $3d$ transition metals are pronouncedly asymmetric. Considering the basic Lorentzian shape of emission lines it was proposed to fit the shape of those asymmetric lines empirically by a superposition of several Lorentzians. The high precision achievable by this approach was already demonstrated for the Cu $K\alpha$ and the Cu $K\beta$ spectra [5,8,9]. Each Lorentzian i is represented by three parameters: the position of the maximum E_i, the relative (compared to the maximum of the emission line) peak intensity I_i, and the full width at half maximum W_i. For a fit of the measured lines a linear background (parameters A and B) has to be taken into account. Consequently the ''true'' (i.e., after the correction for the instrumental broadening) emission spectrum $S(E)$ is represented by

$$S(E)=\sum_{i=1}^{n}\frac{I_i}{1+[(E-E_i)/W_i]^2}+BE+A. \tag{1}$$

In the first step of the fit the number n and the parameters of the Lorentzians are selected manually to start the numerical refinement with optimal initial values of the parameters. This process starts always with the assumption of a doublet for $K\alpha$ and for $K\beta$. The number of Lorentzians is increased in steps of 1 until either the integrated intensity of the last Lorentzian added is smaller than 1% of the integrated intensity of the entire emission line or the differences between measured and fitted profile over the entire energy range are smaller than the standard deviation 2σ given by the measurement statistics.

In the second step of the fit the approximate values of the parameters for each Lorentzian and the background are numerically refined using the Levenberg-Marquard algorithm [22]. The standard approach is slightly modified to improve the convergence of the fit. An optimization cycle is divided into n subcycles. In every subcycle the parameters of only a single Lorentzian are refined and fitted to an ''artificial'' profile. It is constructed by removing the contributions of $n-1$ Lorentzians (except the one to be optimized in this cycle) from the measured profile. The convergence limit achieved is determined by the weighted sum of squares ε:

$$\varepsilon=\sum_{i=1}^{m}\frac{1}{M_i}[F_i(E_i,A,B,I_1,E_{01},W_1,\ldots,I_n,E_{0n},W_n) - M_i(E_i)]^2. \tag{2}$$

M_i is the measured intensity and F_i is the intensity of the fit profile, i.e., a function of the parameters of all Lorentzians and the background for each of the m points of the experimental emission line profile. This convergence criterion takes into account relative deviations between the measured and the modeled profiles and is also sensitive to small (absolute) deviations between the measured and the fitted profiles at the background level, i.e., it gives a higher sensitivity to a correct background determination. The precision of the fit is characterized by the weighted R factor R_w, defined as [23]

$$R_w=\left[\frac{\sum_{i=1}^{n} w_i[F_i(\text{obs})-F_i(\text{calc})]^2}{\sum_{i=1}^{n} w_i F_i(\text{obs})^2}\right]^{1/2}.$$

Here the weighting variable $w_i=1/\sigma_i^2$ and σ_i^2 is the variance due to the counting statistics. F_i(obs) and F_i(calc) are corresponding values on the measured and calculated lineshapes, respectively. The complete set of parameters for a multiple Lorentzian representation of the emission line shapes of Cr, Mn, Fe, Co, Ni, and Cu are given in Tables II and III together with the R_w values. The accuracy of the fits is better for the $K\alpha$ doublet ($R_w \leqslant 1.1\%$) than for the $K\beta_{1,3}$ line ($R_w \leqslant 2.1\%$). The worst fit is obtained for Fe $K\beta$ with $R_w=2.1\%$. Examples for the fits of the $K\alpha_{1,2}$ and $K\beta_{1,3}$ emission lines of Cr, Fe, and Ni are presented in Fig. 1. The high quality of the fit can be seen by the small and nonsystematic residuals. The largest deviations between the measured and fitted profiles are obtained at the maximum, usually with the fitted intensity being higher than the measured one. The small regular oscillations, observed in the tails of some of the emission lines, are obvious relics of the Fourier deconvolution procedure.

The values presented in Tables II and III allow a simple and accurate analytic representation of the most frequently used x-ray emission lines from x-ray tubes. In this empirical decomposition no attempt was made to take into account the physical origin of the asymmetry of these emission lines. A successful physical interpretation of the observed asymmetry was already published [5] for Cu. A similar study for the other lines presented here is in progress.

C. Absolute wavelength determination

The basic problem of high-precision x-ray spectroscopy is the extension of the metric (or, now, the electromagnetic) scale to the x-ray wavelengths [24]. Tabulations for x-ray $K\alpha$ and $K\beta$ emission line wavelengths have existed for several decades (cf. Bearden [25], whose data are identical with the data in Vol. IV of [23]) and the wavelengths or energies, respectively, are quoted with precisions extending down to the ppm level. However, it must be noted that in almost all cases this is only a *relative* precision, taking into account only the accuracy of the angular position through the Bragg law. As x-ray wavelength determination invariably involves crystal diffraction, an accurate determination of the absolute wavelength on a metric scale requires that the lattice parameters of the crystal be known on an absolute metric scale to an accuracy higher than that of the wavelength to be determined. Almost all of the tabulated values [23,25] are based on measurements that do not fulfill this requirement and are likely to be in error by more than 10^{-5} on an absolute scale. The origin of this relatively low accuracy was for a long time the lack of a proper absolute ''ruler'' for atomic-scale length measurements. In the last 10–20 years extensive efforts were made at several national standards institutes, in particular at

TABLE II. Positions E_i, widths W_i, amplitudes I_i, and integrated intensities I_{int} obtained for the individual Lorentzians from a fit of each measured line by the sum of the minimal number of Lorentzians that provides a reasonable fit to the data. Weighted R factors obtained for the fits are also shown.

			$K\alpha_1$					$K\alpha_2$		
	Peak	E_i (eV)	W_i (eV)	I_i	I_{int}	Peak	E_i (eV)	W_i (eV)	I_i	I_{int}
Cr	α_{11}	5414.874(2)	1.457(2)	0.822(2)	0.378	α_{21}	5405.551(3)	2.224(4)	0.386(1)	0.271
	α_{12}	5414.099(6)	1.760(7)	0.237(2)	0.132	α_{22}	5403.986(3)	4.740(50)	0.036(1)	0.054
	α_{13}	5412.745(16)	3.138(20)	0.085(1)	0.084					
	α_{14}	5410.583(30)	5.149(51)	0.045(1)	0.073					
	α_{15}	5418.304(38)	1.988(58)	0.015(1)	0.009					
R_w						1.1%				
Mn	α_{11}	5898.853(2)	1.715(2)	0.790(2)	0.353	α_{21}	5887.743(3)	2.361(5)	0.372(2)	0.229
	α_{12}	5897.867(6)	2.043(7)	0.264(2)	0.141	α_{22}	5886.495(13)	4.216(21)	0.010(1)	0.110
	α_{13}	5894.829(22)	4.499(33)	0.068(1)	0.079					
	α_{14}	5896.532(15)	2.663(20)	0.096(1)	0.066					
	α_{15}	5899.417(17)	0.969(20)	0.007(3)	0.005					
R_w						1.1%				
Fe	α_{11}	6404.148(2)	1.613(3)	0.697(2)	0.278	α_{21}	6391.190(4)	2.487(6)	0.339(1)	0.207
	α_{12}	6403.295(4)	1.965(5)	0.376(2)	0.182	α_{22}	6389.106(22)	2.339(19)	0.060(1)	0.066
	α_{13}	6400.653(19)	4.833(26)	0.088(1)	0.106	α_{23}	6390.275(33)	4.433(12)	0.102(1)	0.065
	α_{14}	6402.077(12)	2.803(15)	0.136(1)	0.094					
R_w						0.9%				
Co	α_{11}	6930.425(2)	1.795(2)	0.809(2)	0.378	α_{21}	6915.713(3)	2.406(4)	0.314(1)	0.197
	α_{12}	6929.388(6)	2.695(8)	0.205(1)	0.144	α_{22}	6914.659(7)	2.773(10)	0.131(1)	0.095
	α_{13}	6927.676(12)	4.555(15)	0.107(1)	0.127	α_{23}	6913.078(23)	4.463(35)	0.043(1)	0.050
	α_{14}	6930.941(27)	0.808(27)	0.041(2)	0.088					
R_w						0.5%				
Ni	α_{11}	7478.281(2)	2.013(2)	0.909(2)	0.487	α_{21}	7461.131(4)	2.674(5)	0.351(1)	0.250
	α_{12}	7476.529(13)	4.711(15)	0.136(1)	0.171	α_{22}	7459.874(15)	3.039(21)	0.079(1)	0.064
						α_{23}	7458.029(48)	4.476(78)	0.024(1)	0.028
R_w						1.0%				
Cu	α_{11}	8047.837(2)	2.285(3)	0.957(2)	0.579	α_{21}	8027.993(5)	2.666(7)	0.334(1)	0.236
	α_{12}	8045.367(22)	3.358(27)	0.090(1)	0.080	α_{22}	8026.504(14)	3.571(23)	0.111(1)	0.105
R_w						0.7%				

the National Institute of Standards and Technology, Gaithersburg (MD) [26,27] and the Physikalisch-Technische Bundesanstalt, Braunschweig (Germany) [12(a)] but also in Japan [12(b)] and Italy [12(c)], to bridge the gap in absolute wavelength determination between optical and x-ray wavelengths. A combined x-ray and light interferometric method capable of measuring lattice parameters on an absolute metric scale to a relative accuracy of 10^{-7} or better was developed and the lattice parameter of highly pure silicon crystals were determined [12,26,27]. The silicon crystal used in our measurement was calibrated based on such a measurement.

To date, only a few x-ray wavelengths were determined on an absolute scale using such calibrated crystals to an accuracy $\Delta\lambda/\lambda \approx 10^{-6}$. The value with the highest accuracy is that of the Cu $K\alpha_1$, which was measured to an accuracy of [16] $\Delta\lambda/\lambda \approx 3\times10^{-7}$. The data presented here are, to our knowledge, the first set of systematic absolute wavelength measurements of the $3d$ transition metal emission lines with a comparable precision.

The general strategy for the determination of the wavelengths is presented in Sec. II B. The measured maximum positions of the $K\alpha_{1,2}$ and the $K\beta_{1,3}$ lines are listed in Table IV, along with those from the widely used tabulation of Bearden [25]. These data are presented in the original notation, using the Å* unit and the probable error (p.e.). They are also converted to SI units in the next column using $\lambda(\text{nm}) = \lambda(\text{Å*})0.10001481(92)$ of the 1986 CODATA least-squares adjustment [85] with the error listed as one standard deviation (1.48p.e.). As can be seen, our values are systematically larger than the original values of Bearden (with the exception of Fe and Co $K\alpha_2$, which have negative deviations smaller than 4×10^{-6}) by an amount ranging up to 2.42×10^{-5} (Cu $K\alpha_2$). A large part of the deviation is, of course, due to Bearden's use of the x-unit, rather than the

TABLE III. Same as Table II, but for the $K\beta_{1,3}$ spectra. The weighted R factors here are 1.5–2 times worse than those obtained for the $K\alpha$ spectra.

		$K\beta_{1,3}$			
	Peak	E_i (eV)	W_i (eV)	I_i	I_{int}
Cr	β_a	5947.00(1)	1.70(1)	0.670(5)	0.307
	β_b	5935.31(9)	15.98(21)	0.055(1)	0.236
	β_c	5946.24(1)	1.90(2)	0.337(5)	0.172
	β_d	5942.04(5)	6.69(8)	0.082(1)	0.148
	β_e	5944.93(3)	3.37(4)	0.151(2)	0.137
R_w			1.7%		
Mn	β_a	6490.89(1)	1.83(1)	0.608(5)	0.254
	β_b	6486.31(7)	9.40(9)	0.109(2)	0.234
	β_c	6477.73(8)	13.22(15)	0.077(1)	0.234
	β_d	6490.06(2)	1.81(2)	0.397(5)	0.164
	β_e	6488.83(3)	2.81(4)	0.176(4)	0.114
R_w			1.6%		
Fe	β_a	7046.90(9)	14.17(17)	0.107(2)	0.301
	β_b	7057.21(2)	3.12(2)	0.448(5)	0.279
	β_c	7058.36(1)	1.97(2)	0.615(7)	0.241
	β_d	7054.75(6)	6.38(8)	0.141(3)	0.179
R_w			2.1%		
Co	β_a	7649.60(8)	3.05(1)	0.798(4)	0.449
	β_b	7647.83(3)	3.58(3)	0.286(4)	0.189
	β_c	7639.87(8)	9.78(12)	0.085(1)	0.153
	β_d	7645.49(6)	4.89(8)	0.114(3)	0.103
	β_e	7636.21(20)	13.59(37)	0.033(1)	0.082
	β_f	7654.13(11)	3.79(16)	0.035(2)	0.025
R_w			1.6%		
Ni	β_a	8265.01(1)	3.76(2)	0.722(4)	0.450
	β_d	8263.01(2)	4.34(3)	0.358(4)	0.258
	β_c	8256.67(10)	13.70(16)	0.089(1)	0.203
	β_d	8268.70(7)	5.18(9)	0.104(3)	0.089
R_w			1.9%		
Cu	β_a	8905.532(2)	3.52(1)	0.757(3)	0.485
	β_b	8903.109(10)	3.52(1)	0.388(2)	0.248
	β_c	8908.462(20)	3.55(3)	0.171(2)	0.110
	β_d	8897.387(50)	8.08(8)	0.068(1)	0.100
	β_e	8911.393(57)	5.31(8)	0.055(2)	0.055
R_w			1.0%		

true SI standard, not available to him at that time. The SI converted Bearden data shows a much better agreement with our data, with almost random deviations. Nevertheless, upon careful examination a mean deviation of -4.6×10^{-6} is observed between Bearden's set and ours, possibly due to a small remnant systematic deviation in the conversion factor. Thus, the present results provide a large set of accurate, well calibrated x-ray wavelengths, which should prove useful for a variety of precision measurements involving x rays.

D. Linewidth and index of asymmetry

1. Introduction

A frequently used and convenient (but not very accurate) quantification of the line shape is by its full width at half maximum (FWHM) and its index of asymmetry. Both values allow a comparison with other experimental results and a general classification of our measurements in relation to other reference data. Note, however, that the line shape can-

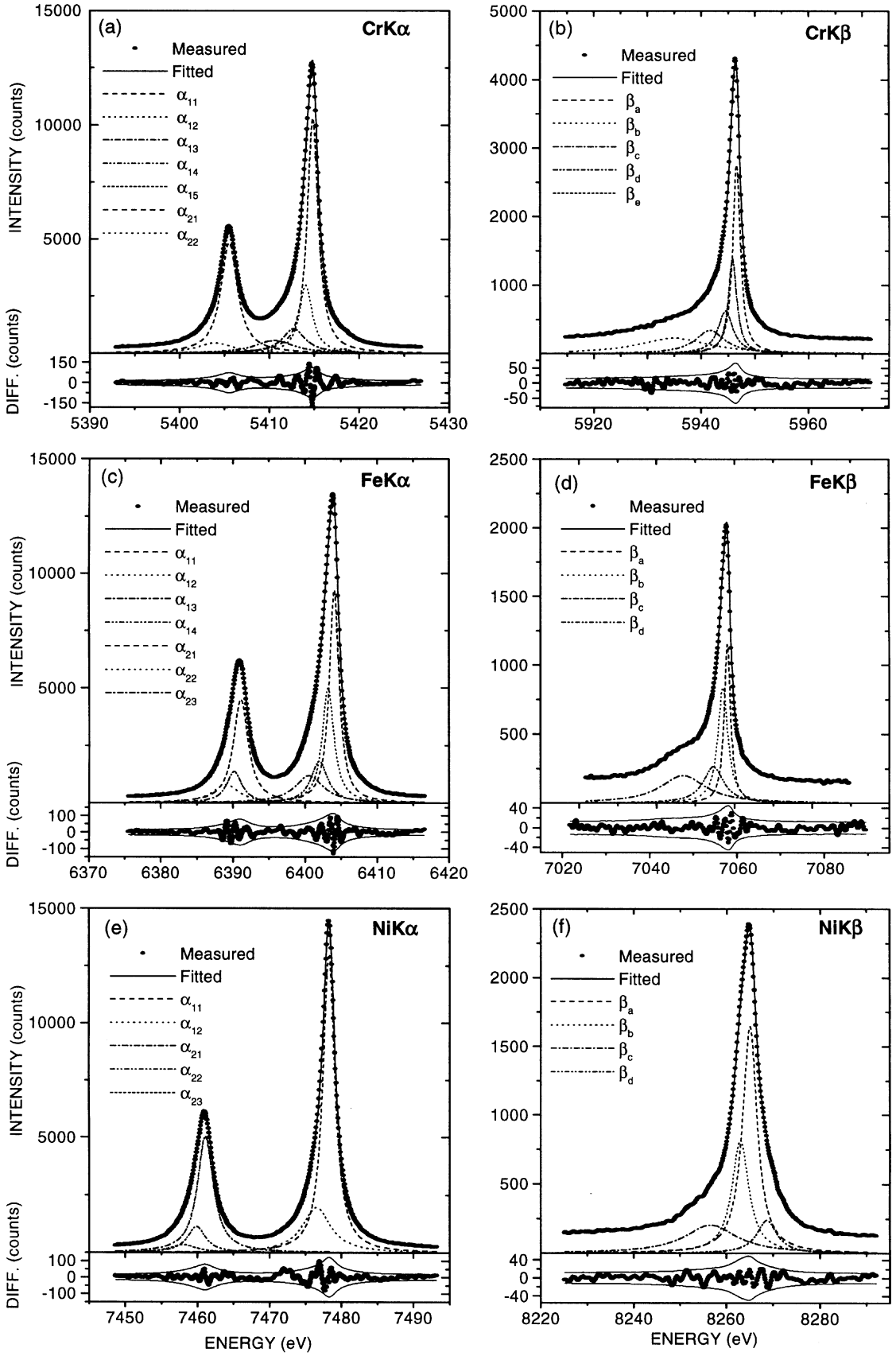

FIG. 1. Measured $K\alpha$ and $K\beta$ emission lines of Cr (a),(b), Fe (c),(d), and Ni (e),(f) (points). A fit by a sum of a minimal set of Lorentzians (solid line) is also shown for each line, along with the individual Lorentzians of the set (dashed lines). The fit parameters are given in Tables II and III. The fit residuals (DIFF) are shown under each spectrum, with thin lines denoting the $\pm 2\sigma$ values of the data, where σ is the standard deviation due to the counting statistics.

TABLE IV. The peak wavelengths of the measured lines, on an absolute metric scale. Measurement uncertainties are given in brackets, and the widely used values of Bearden [23,25], listed in Å* with their probable error (pe) values, are also shown. The fourth column shows these values in nm units, using the relation λ (nm) = λ (Å*)0.100 001 481 [85] and the standard deviation 1.48×pe. Note the part-per-million level of accuracy of the present results.

Line	Reflection *hkl*	λ_{Bearden} (Å*)	Corr. λ_{Bearden} (nm)	λ (nm) (this work)	*E* (eV) (this work)
Cr $K\alpha_1$	331	2.289 70(2)	0.228 973(3)	0.228 972 6(3)	5414.81(1)
Cr $K\alpha_2$		2.293 606(3)	0.229 364 0(5)	0.229 365 1(3)	5405.54(1)
Cr $K\beta_{1,3}$		2.084 87(2)	0.208 490(3)	0.208 488 1(4)	5946.82(1)
Mn $K\alpha_1$	422	2.101 820(9)	0.210 185(2)	0.210 185 4(3)	5898.80(1)
Mn $K\alpha_2$		2.105 78(2)	0.210 581(3)	0.210 582 2(3)	5887.59(1)
Mn $K\beta_{1,3}$	333	1.910 21(2)	0.191 024(3)	0.191 021 6(4)	6490.18(1)
Fe $K\alpha_1$	333	1.936 042(9)	0.193 607(2)	0.193 604 1(3)	6404.01(1)
Fe $K\alpha_2$		1.939 980(9)	0.194 001(2)	0.193 997 3(3)	6391.03(1)
Fe $K\beta_{1,3}$		1.756 61(2)	0.175 664(3)	0.175 660 4(4)	7058.18(3)
Co $K\alpha_1$	531	1.788 965(9)	0.178 899(2)	0.178 899 6(1)	6930.38(1)
Co $K\alpha_2$		1.792 850(9)	0.179 288(2)	0.179 283 5(1)	6915.54(1)
Co $K\beta_{1,3}$	620	1.620 79(2)	0.162 081(3)	0.162 082 6(3)	7649.45(1)
Ni $K\alpha_1$	620	1.657 910(8)	0.165 794(2)	0.165 793 0(1)	7478.26(1)
Ni $K\alpha_2$		1.661 747(8)	0.166 177(2)	0.166 175 6(1)	7461.04(1)
Ni $K\beta_{1,3}$	444	1.500 135(8)	0.150 016(2)	0.150 015 2(3)	8264.78(1)
Cu $K\alpha_1$	444	1.540 562(2)	0.154 058 5(3)	0.154 059 29(5)	8047.83(1)
Cu $K\alpha_2$		1.544 390(2)	0.154 441 3(3)	0.154 442 74(5)	8027.85(1)
Cu $K\beta_{1,3}$	553	1.392 218(9)	0.139 224(2)	0.139 223 4(6)	8905.42(4)

not be described precisely by a simple asymmetric profile in all cases. Such an approximation is quite good for the $K\alpha_{1,2}$ lines but a very bad one for the $K\beta_{1,3}$ line, where a substructure due to the two unresolved lines of the doublet, the $K\beta_1$ and $K\beta_3$ lines, separated by less than their combined half widths, is clearly visible (see Fig. 1). Thus, we have avoided assigning an index of asymmetry to the $K\beta_{1,3}$ lines.

In our measurements the FWHM and the index of asymmetry were determined from the background-corrected Lorentzian fits (see above). The index of asymmetry is defined as the ratio of the half widths at half height on the low and high energy sides of the peak [28]. In Table V the FWHM of $K\alpha_1$, $K\alpha_2$, $K\beta_{1,3}$ and the index of asymmetry for $K\alpha_1$, $K\alpha_2$ are presented. The experimental uncertainties in the values cited in the table were determined taking into account multiple measurements and multiple fits of each spectrum. They are always <0.05 eV for the FWHM. The errors for the index of asymmetry are <0.05 eV for $K\alpha_2$ and <0.07 eV for $K\alpha_1$. The FWHM and the index of asymmetry are compared in Figs. 2 and 3 with available previous measurements, not for all of which error estimates are available.

2. The Kα linewidths

As can be seen in Fig. 2, the previous measurements of the FWHM values are rather broadly scattered, reaching a factor of two in extreme cases [Cr $K\alpha_1$ in Fig. 2(a)]. Furthermore, the deviations exceed the error bars, in the few cases where these are available, indicating probable systematic errors. Also, a tendency of ''clustering'' is observed for

TABLE V. The full width at half maximum (FWHM), index of asymmetry, and corrected integrated intensity ratios for the measured spectra.

	FWHM (eV)			Index of asymmetry		$I(K\alpha_2)/I(K\alpha_1)$	$I(K\beta_{1,3})/I(K\alpha_{1,2})$
	$K\alpha_1$	$K\alpha_2$	$K\beta_{1,3}$	$K\alpha_1$	$K\alpha_2$		
Cr	1.88	2.52	2.53	1.38	1.01		0.139
Mn	2.47	2.92	2.97	1.49	1.17	0.51	0.139
Fe	2.55	3.14	3.53	1.66	1.24	0.51	0.144
Co	2.33	3.18	4.37	1.38	1.33	0.52	0.137
Ni	2.24	3.16	5.40	1.18	1.21	0.52	0.147
Cu	2.35	3.41	5.92	1.07	1.36	0.52	0.141

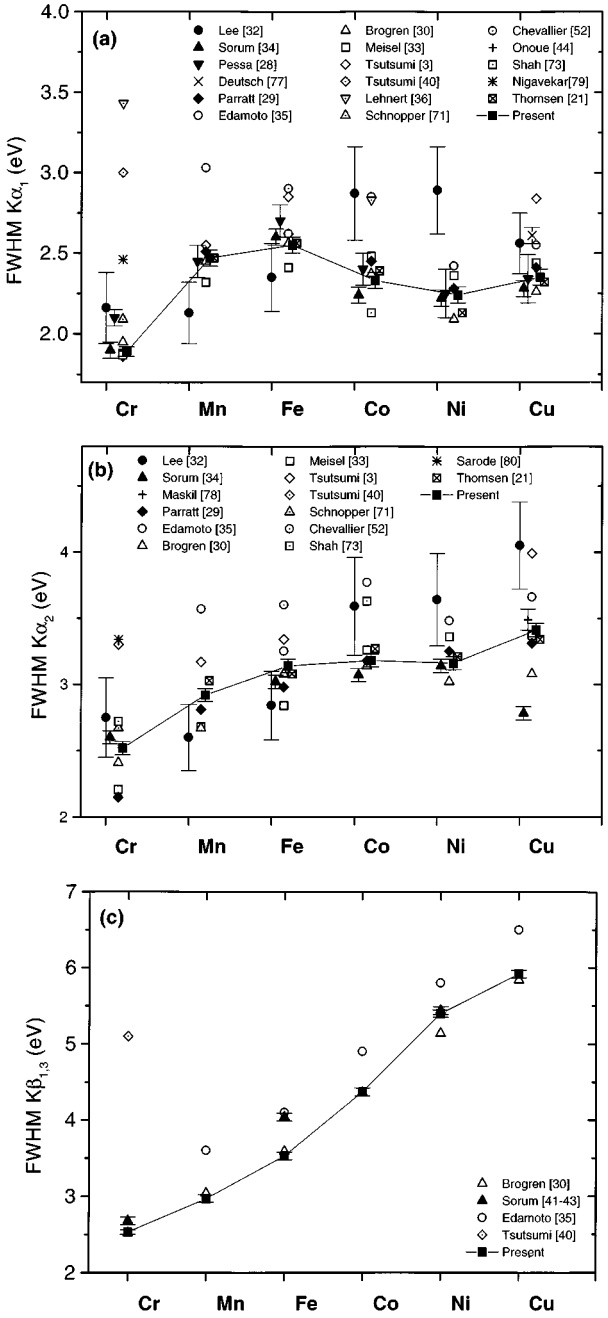

FIG. 2. The width (FWHM) of $K\alpha_1$ (a), $K\alpha_2$ (b) and $K\beta$ (c) lines of Cr, Mn, Fe, Co, Ni, and Cu, as derived from previous studies (listed in the legend by first author name and reference number) and the present measurements. Note the weak maximum near Fe for the $K\alpha$ lines and the monotonic increase with Z for the $K\beta$ lines.

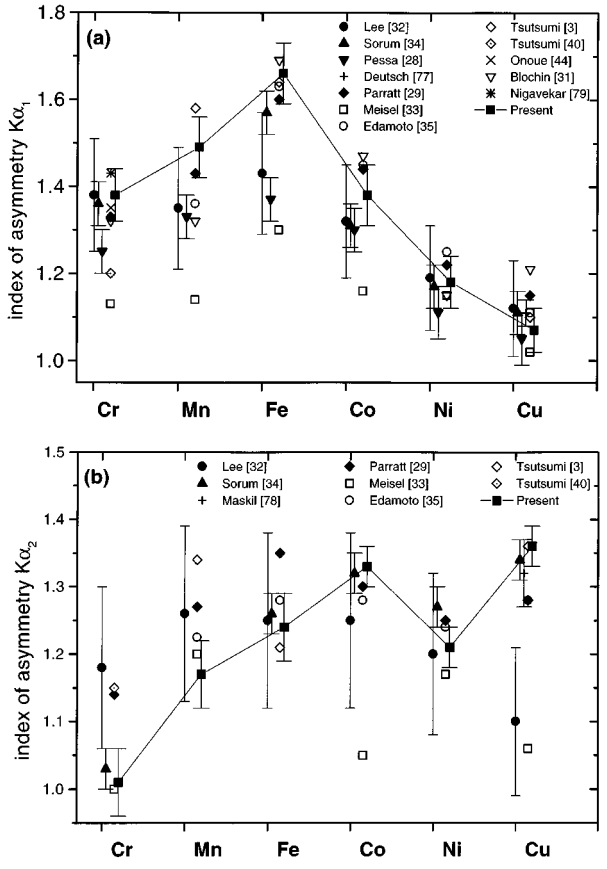

FIG. 3. Asymmetry indices for the $K\alpha_1$ (a) and $K\alpha_2$ (b) lines of Cr, Mn, Fe, Co, Ni, and Cu, derived from the present measurements and previous studies.

most of the data points with a few obvious ''runaway'' points. The fact that most of the previous measurements yield higher values for the widths than ours indicates a probable neglect of, or incomplete correction for, the instrumental broadening. Only few of the previous data were corrected for an instrumental broadening, although it was realized early that the instrumental broadening has a significant effect [29] and even simple corrections can lead to a significant improvement in the results. The ''true'' FWHM of the emission line can be determined by a simple subtraction of the FWHM of the spectrometer window from the FWHM of the measured emission line [29–31]. This approach is exact if both the emission line profile and instrumental function have a Lorentzian shape. Normally this is not the case. For emission lines with an obvious asymmetric shape it becomes less exact but still gives a reasonable approximation even for the $K\beta$ line shapes [29–31]. The combined fit and deconvolution method of Lee and Salem [32] seems to disagree with the general Z-dependent trend of all other measurements shown in Figs. 2(a) and 2(b).

Our experience indicates that the determination of the FWHM and the index of asymmetry is especially sensitive to a precise correction for the instrument broadening. In the case of an optimally adjusted spectrometer the instrument function is nearly symmetric and narrow (see [8]). A ''broad'' symmetric instrumental function tends to suppress the line asymmetry and give systematically too small values for the index of asymmetry. This effect cannot be corrected after the measurement. Only experiments with a narrow spectrometer window in an optimized spectrometer setup provide a precise determination of the index of asymmetry and the FWHM. Our data are determined with the same optimized spectrometer setup and with a well-defined correction procedure for the narrow spectrometer window. They have a higher accuracy than most of the other reference data (see error bars in Figs. 2 and 3). Additionally they fit into the above-mentioned ''clusters'' and present the same general Z-dependent trends as the other more comprehensive refer-

ence data [28–31,33,34]. General trends for the Z dependence of the FWHM and the index of asymmetry for the $3d$ transition metals are therefore deduced in the following using our data.

The FWHM of the $K\alpha$ lines show a good agreement with most of the previous data. Some of these are systematically too large, as those of Edamoto [35] and Lehnert [36]. The good correspondence with the early data of Parratt [29], which were corrected for resolution effects, show the effectivity of even a simple correction procedure. Good agreement is also found with the measurements of Bearden [37] as analyzed by Thomsen [21]. In addition, the Z-dependent trend of the more comprehensive data sets [28–30,33,34] agree with those in our data. Generally the FWHM of the $K\alpha_1$ line increases from Cr to Fe, has a distinct local minimum for Ni and increases once more for Cu. This trend is the same for the FWHM of the $K\alpha_2$ line although there a plateau is observed in the Fe-Ni region rather than a distinct minimum. The FWHM of the $K\alpha_2$ line is larger than that of the $K\alpha_1$ line by 0.5–1 eV. This can be accounted for by the reduced lifetimes due to the L_2-$L_3M_{4,5}$ Coster-Kronig transition, which is forbidden in the free atom but allowed in the solid [6,38,39].

3. The Kβ linewidths

For the FWHM of $K\beta_{1,3}$ the number of available previous data is rather limited [30,35,40–43]. They are presented in Fig. 2(c). Their agreement with our data is even better than for the $K\alpha$ widths. This is most probably due to the fact that the considerably larger FWHM of the line reduces the relative contribution of the instrumental broadening. Nevertheless, the early data of Edamoto [35] and Tsutsumi [40] are systematically larger than recent measurements. This results most probably from instrumental effects. Unlike the $K\alpha$ lines the FWHM of the $K\beta_{1,3}$ peak increases monotonically from Cr to Cu, indicating that the nonmonotonic behavior of the $K\alpha$ widths is probably due to the behavior of the L level widths rather than the K level ones. The smaller overlap of the M and K wave functions, as compared to the K and L ones, may reduce the relative influence of possible similar-sized nonmonotonic contributions originating in the final state level widths.

4. Index of asymmetry of the Kα lines

Our results and previous data for the index of asymmetry are presented in Figs. 3(a) and 3(b) for $K\alpha_1$ and $K\alpha_2$, respectively. The spread of the data is large, probably due to the high sensitivity of the index of asymmetry to the width of instrumental function as mentioned above. A broad instrumental function should result in a systematically too low asymmetry. The data of Meisel [33] and Pessa [28] for the narrow and highly asymmetric $K\alpha_1$ line indeed show this tendency; they are systematically smaller than the majority of the other measurements in Fig. 3(a). It is clear from the results that the asymmetry is generally larger for the $K\alpha_1$ peak. Our indices of asymmetry for the $K\alpha_1$ peak are larger than most of the other data. This is particularly true for Mn, Fe, and Co, which have the highest asymmetry among the $3d$ transition elements. Our results agree well with those of Blochin [31], Sorum [34], and the high-resolution measurements of Onoue and Suzuki [44]. The spread in the reported values of the index of asymmetry is even larger for the $K\alpha_2$ line than for the $K\alpha_1$ as shown in Fig. 3(b). Despite the large spread, a general trend for the Z dependence of the index can be observed. For $K\alpha_1$ a distinct maximum occurs for Fe, with the index decreasing monotonically towards both Cr and Cu. This maximum coincides with the maximum in the FWHM, shown in Fig. 2(a). The Z dependence of the asymmetry of $K\alpha_2$ peak shows two characteristic deviations from $K\alpha_1$. The maximum asymmetry is shifted to Co and there exists a distinct minimum for Ni, which does not occur for $K\alpha_1$. The asymmetry increases once more for Cu. Both the maximum for Co and the minimum of the asymmetry for Ni are confirmed by most of the other measurements and should be, therefore, considered to be real effects.

5. Z-dependent trends

Several attempts have been made in the past to give a physically motivated, or even a purely empirical functional representation for the experimentally observed Z dependence of the lines' characteristic parameters, such as the width, asymmetry index, etc., over a broad Z range, for use in practical applications. These attempts were successful for the widths [33,45] and the $K\alpha$ doublet separation [46]. However, distinct deviations between the smooth representation and the measured values were observed in all these forms for $20 \leqslant Z \leqslant 30$, i.e., in the region of the $3d$ transition metals (and, to a smaller extent, also for the $4d$ transition elements). In this Z range the measured widths exceed significant the widths extrapolated from lower- and higher-Z elements. These deviations were ascribed to the unique electronic structure of the atoms in this range, which have a partly or fully populated $4s$ shell and an open $3d$ shell, giving rise to complicated transition structures in the x-ray emission process. Similar anomalous deviations were observed in the XPS linewidths of the same elements [39,47]. Finster [4] and Pessa [28] attempted to correlate these deviations with the number of unpaired $3d$ electrons in the atom, as calculated by them. While neither calculation result in an accurate correspondence, they show a reasonable qualitative correlation with the Z dependence of the deviations. In particular, the number of unpaired electrons is maximal for iron, which corresponds well to the experimentally observed maxima of the FWHM for $K\alpha_1$ and $K\alpha_2$ and for the maximum of the index of asymmetry for $K\alpha_1$.

Tsutsumi [3] proposed that the anomalous widths and asymmetric line-shape results from an exchange interaction between electrons of the incomplete $3d$ shell and those of the $2p$ shell, left open by the x-ray emission process. This will split the L levels into two sublevels each, and, thus, also each of the $K\alpha$ lines into two close lines. Since the separation of the two lines is smaller than their combined widths and their intensities are unequal, the splitting will yield the skewed line shapes observed. While this model leads to a qualitative improvement in the line-shape fits, and hence also of the widths, the theoretically expected splitting is usually too small to explain the experimentally observed asymmetry and width. Furthermore, it predicts symmetrical line shapes for atoms having complete $3d$ shells, like Cu, in obvious contradiction with the measurements [48]. XPS measurements [39,49,50] demonstrated that the excess width of the x-ray

lines results from a broadening of the L_{II} and L_{III} levels beyond their intrinsic lifetime widths due to strong Coster-Kronig (CK) transitions. These are allowed in the solid phase, though energetically forbidden in the isolated atom (gas phase) case [39]. The inclusion of the CK transition greatly improves the agreement of the total line shape and its width with the experiment. Pease [51], however, showed, based on measured soft x-ray emission spectra of the $\underline{2p} \rightarrow \underline{3s}$ transition, that the CK transitions are insufficient to account for the L level widths over the full $20 \leqslant Z \leqslant 30$ range, and that additional (unspecified) nonlifetime effects need to be included.

Clearly, the simplified approach of addressing only the width and asymmetry of a line, is insufficient to account for the shapes of complex spectra such as those of the $3d$ transition metals. Thus, attempts have been made to fit the full emission spectrum by a model based on various *ab initio*, or semiempirical, calculated transition arrays. Using relativistic Dirac-Fock *ab initio* calculations and high-resolution spectral measurements, we have shown recently [5] that both the Cu $K\alpha$ and Cu $K\beta$ emission spectra could be accurately reproduced assuming contributions from two transitions only: the diagram $\underline{1s} \rightarrow \underline{lp}$ and the $\underline{3d}$ spectator hole $\underline{1s3d} \rightarrow \underline{lp3d}$, where $l=\underline{2,3}$ for the $K\alpha$ and the $K\beta$ lines, respectively. The validity of this approach is further supported by observations of a strong energy dependence of the Fe $K\alpha$ [52] and Ar $K\beta$ [53] emission line shape on the exciting photon energy when photoexcited close to the K edge. For photons with insufficient energy to excite the initial $\underline{1s3d}$, but sufficient to do so for the lower-energy $\underline{1s}$ hole state, a much more symmetric and narrower line is observed. An analysis of the emission lines of $3d$ transition metals other than Cu, based on Dirac-Fock *ab initio* calculations, as well as excitation energy-dependent measurements of emission spectra near threshold are in progress [7].

E. The $K\alpha_2/K\alpha_1$ and $K\beta_{1,3}/K\alpha_{1,2}$ integrated intensity ratios

The accurate knowledge of the $K\alpha_2/K\alpha_1$ and the $K\beta_{1,3}/K\alpha_{1,2}$ integrated intensity ratios is required for a number of practical applications of x rays, e.g., structure determination from powder diffraction patterns, like the Rietveld refinement technique, etc. In precision single crystal structure refinement methods a quantitative analysis of the intensity of a large number of reflections is required, over a large Bragg angle range. Intensity contributions from simultaneously excited characteristic emission lines, i.e., from the $K\alpha$ doublet and/or the $K\alpha,\beta$ lines for a particular reflection cannot always be resolved experimentally. This is particularly true for small Bragg angles. The determination of the quantitative contribution of each emission line to the measured reflection requires, in this case, an accurate foreknowledge of the intensity ratios $K\alpha_2/K\alpha_1$ and $K\beta_{1,3}/K\alpha_{1,2}$. Finally, these ratios depend sensitively on the atomic structure. Thus they have been widely used also for critical evaluation of atomic structure model calculations. We now discuss the values of these ratios as obtained in our measurements.

1. The $K\alpha_2/K\alpha_1$ integrated intensity ratio

Our results, along with previous measurements, are plotted in Fig. 4. The $K\alpha$ doublet transition is a special case of a multiplet transition. Applying the Burger-Dorgelo-Ornstein rule [20] to this doublet an intensity ratio of 0.5 is expected. This value should be independent of the atomic number Z. The early measurements of Williams [54] for a selection of twenty elements from $Z=24$ to $Z=52$ confirm these predictions. The results are statistically distributed and the average $K\alpha_2/K\alpha_1$ intensity ratio is determined to be 0.5003. Later theoretical calculations [55] taking into account exchange interactions presented slightly larger and also weakly Z-dependent values. These results are supported quantitatively by the experimental observations of McCrary [56] and Salem [57,58], which also obtained values slightly larger than 0.5 for the $K\alpha_2/K\alpha_1$ intensity ratio. To the best of our knowledge, more recent experimental studies of the $K\alpha_2/K\alpha_1$ intensity ratio of the $3d$ transition metals are not available in the literature. For a verification of the theoretically predicted small deviations of $K\alpha_2/K\alpha_1$ intensity ratio from 0.5 precise corrections of the measured intensities are necessary. This is especially true for the energy-dependent integrated reflectivity of the crystal, which can be calculated from the dynamical theory of x-ray diffraction [59], the energy-dependent absorption of the radiation in the target itself, and the intensity contributions from satellite transitions included in the doublet lines (see, for example, [5]).These energy-dependent corrections are small for the $K\alpha_2/K\alpha_1$ intensity ratio, since the energies of both doublet lines are only slightly different. They are considerably larger for the $K\beta_{1,3}/K\alpha_{1,2}$ intensity ratio as we discuss below.

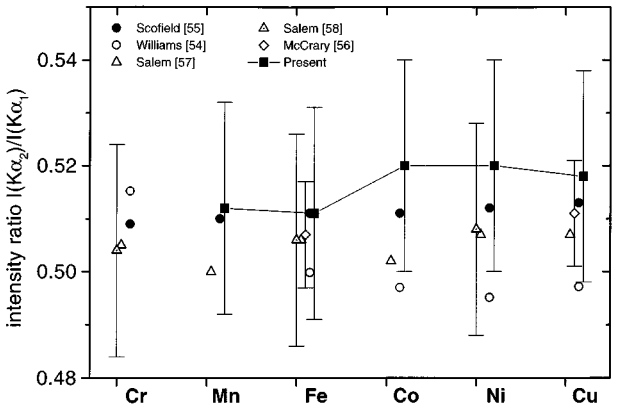

FIG. 4. The $K\alpha_2/K\alpha_1$ intensity ratio, as obtained in the present measurements and previous studies. No reliable value could be derived from the present measurements for Cr, for reasons detailed in the text.

A more serious problem for the accurate determination of the $K\alpha_2/K\alpha_1$ intensity ratio is the partitioning of the intensity of the spectrum between the two lines. The intensity between the doublet lines is nonzero and thus its assignment is done using additional assumptions, such as an identical peak shape and/or a fixed ratio of the FWHM of the doublet peaks [56]. These assumptions are not universally valid, particularly in our case where the shapes of the $K\alpha_1$ and the $K\alpha_2$ peaks are significantly different (see Table V). The differences are especially large for Mn, Fe, and Co.

In our experiments the energy-dependent corrections of the integrated intensity and the absorption are performed according to [8]. The intensity assignment to each of the doublet peaks is done using the results of the decomposition of

the doublet into single Lorentzians. The intensity of each doublet peak is the sum of all Lorentzians included in this peak. The results are shown in Fig. 4. They show a very good agreement with the theoretical predictions for Mn and Fe, while the values determined for Co, Ni, and Cu exceed Scofield's [55] theoretical values by 1–2 %, which are, nevertheless, still within the 2% experimental uncertainties. The intensity partitioning method fails completely for chromium, since the Cr $K\alpha$ doublet in our measurement has a significant intensity in between the two peaks and a unique, objective partitioning of this contribution between the two doublet peaks is not possible. We wish to point out that the $K\alpha_2/K\alpha_1$ intensity ratios in Table V hold for typical excitation conditions of x-ray tubes and therefore can be used in analyzing diffraction and other data measured with such tubes. Also note that both doublet lines include contributions from satellite transitions and an exact determination of the intensity ratio for the diagram transitions $\underline{1s}\rightarrow\underline{2p_{1/2}}$ and $\underline{1s}\rightarrow\underline{2p_{3/2}}$ requires a separation of these satellite contributions using a suitable model for the whole transition array. This was demonstrated for the Cu K emission spectra, where contributions due to spectator transitions of 20–30 % were determined [5]. In that case, both doublet lines were nearly equally contaminated by these satellite intensity contributions and the pure $I(\underline{1s}\rightarrow\underline{2p_{1/2}})/I(\underline{1s}\rightarrow\underline{2p_{3/2}})$ ratio is determined to be 0.53 ± 0.01, which is in good agreement with the value presented in Table V.

2. The $K\beta_{1,3}/K\alpha_{1,2}$ integrated intensity ratio

In contrast to the $K\alpha_2/K\alpha_1$ ratio, almost all published measurements of the $K\beta_{1,3}/K\alpha_{1,2}$ ratio have been done using semiconductor detectors (SD), since the separation of these spectra, 500–900 eV for the transition elements, is considerably larger than the $\sim$200 eV resolution of the SD. We were able to find in the literature only a single experiment using a crystal spectrometer (CS) [58]. This state of affairs is due to the difficulties in correcting the CS-measured data for the various effects discussed above, and, in particular, accounting for the varying reflection properties of the crystal [60]. In spite of this, the CS is preferable in principle to the SD for such measurements due to its much higher resolution, as compared to a SD, which reduces drastically the spurious background due to bremsstrahlung and allows a clear separation of x-ray satellites, such as the $K\alpha_{3,4}$ or the $K\beta_{2,5}$ lines. As shown in the preceding section, the reflection properties of a perfect crystal could be handled numerically. Furthermore, for extracting exact ratios from a SD measured data significant corrections are required as well [61,62]. The energy-dependent efficiency of the SD must be known and the corrections for self-absorption and absorption in windows and air, mentioned below, must also be carried out when using a SD.

The two CS-measured $K\alpha_{1,2}$ and $K\beta_{1,3}$ spectra were recorded during two different runs. To avoid complications the measuring conditions (tube voltage and current, slit widths) remained the same for both runs. The corrections applied to the raw data after the measurements are as follows: the absorption in air and in the Be windows of the x-ray tube and the detector for the different peak emission wavelengths was calculated using absorption coefficients from [14]. The reflection $R_{\rm int}$ of the silicon crystal was calculated using the dynamical theory based computer code DIXI [63].

The background is subtracted from the spectra by least-squares fitting [22] of Lorentzians and a linear background. This is crucial because small changes in the background cause significant changes in the intensity (in the percent range). The last correction concerns the self-absorption of the radiation produced in the x-ray tube anode. Because of the thick target, it is not possible to neglect this effect. We used the approach of Sewell *et al.* [64] who deduced an analytical expression for the correction by using results of tracer experiments. The uncorrected and corrected values for the $K\beta/K\alpha$ intensity ratios, along with the various correction factors, are given in Table VI. The formula for the corrected ratio is

$$\frac{I_{K_\beta}(\mathrm{cor})}{I_{K_\alpha}(\mathrm{cor})}=\frac{I_{K_\beta}(\mathrm{meas})}{I_{K_\alpha}(\mathrm{meas})}\frac{S_\alpha}{S_\beta}\frac{T_\alpha}{T_\beta}\frac{R_\alpha}{R_\beta},$$

where S, T, and R are the self-absorption, the transmission through air and Be, and the integrated reflectivity of the crystal, respectively. Strictly speaking, the measured intensities, $I(\mathrm{meas})$, are given by an integral of the intrinsic, undistorted intensity over the angular and energy spreads of the incoming beam, with each intensity value multiplied by the value of S, T, and R at that energy and incidence angle. Thus, to obtain the corrected intensity values, $I(\mathrm{cor})$, inversion of this integral is required. However, as the angular width of the crystal reflectivity curve is extremely narrow, we have approximated the intensity variation over this range to be constant, thus allowing the integration to be carried out and effective correction factors to be expressed as individual multiplicative factors, yielding the equation above. While this is admittedly an approximation, it should be a very good one, considering the very narrow widths, a few arcsec only, of the reflectivity curves of the perfect silicon crystal used in the measurements. The necessity of these energy-dependent corrections becomes clear when comparing the uncorrected and corrected $K\beta/K\alpha$ intensity ratios listed in the Table VI.

Most of the $K\beta$-emission lines were measured using two different crystal reflections. The Cu $K\alpha$ spectrum was measured with 3 different reflection orders, namely, 333, 444, and 620. These independent measurement allow a better assessment of the measurements the errors, in particular those originating in the crystal parameters. We estimated a precision of better than 4%. By using the same reflection in the $K\alpha$ and $K\beta$ measurements the overall error in the ratio should not exceed 5%, as errors of multiplicative nature cancel. The influence of the energy of the exciting electrons on the $K\beta/K\alpha$ intensity ratio is negligible [65]. A comparison of this ratio for different excitation mechanisms is given by Perujo *et al.* [66].

In Fig. 5 our values are compared with previous results. Only theoretical results and experiments employing electron or photon excitation are included, since the prominent multiple ionization in the case of heavy-ion excitation strongly alters the $K\beta/K\alpha$ intensity ratio [32,67]. Also included in the comparison are theoretical data from Scofield, Manson, and Jankowski. Of the theoretical results, Manson's [68] simple nonrelativistic Hartree-Slater calculations clearly underestimate almost all other experimental and theoretical results. The more sophisticated relativistic Dirac-Fock calcula-

TABLE VI. The raw and corrected $K\beta_{1,3}/K\alpha_{1,2}$ intensity ratio. The correction factors discussed in the text are also listed.

Line and reflection	$I(K\beta)/I(K\alpha)$ raw	Transmission ratio T_α/T_β	Self-absorption ratio S_α/S_β	Reflectivity ratio R_α/R_β	$I(K\beta)/I(K\alpha)$ corrected
Cr $K\alpha$ (331)		0.427	0.869		
Cr $K\beta$ (331)	0.223			1.681	0.139
Cr $K\beta$ (422)	0.417			0.949	0.147
Mn $K\alpha$ (422)		0.512	0.920		
Mn $K\beta$ (422)	0.131			2.354	0.140
Fe $K\alpha$ (333)		0.588	0.929		
Fe $K\beta$ (333)	0.136			1.929	0.143
Fe $K\beta$ (531)	0.231			1.206	0.152
Co $K\alpha$ (531)		0.655	0.931		
Co $K\beta$ (531)	0.066			3.390	0.137
Ni $K\alpha$ (620)		0.713	0.933		
Ni $K\beta$ (620)	0.062			3.573	0.147
Ni $K\beta$ (444)	0.190			1.190	0.150
Cu $K\alpha$ (444)		0.761	0.903		
Cu $K\beta$ (444)				3.391	0.141

tions of Scofield [55] and of Jankowski and Polasik [69], which also include exchange effects, agree much better with the experimental results. The recent results of Kücükönder *et al.* [70] considerably underestimate all other measurements. This may be due to an overcorrection for the particle size of the powdered samples, used in the measurements. As can be seen, our results agree well with most of the other values, except for Fe and Ni, which seem to be too high. In view of the error bars, it is not clear if this is a real effect. We note, however, that Berényi *et al.* [65] also find an enhanced ratio for Ni. Our results are consistently at the upper part of the experimental values' spread, which could hint at a systematic deviation in one of the corrections.

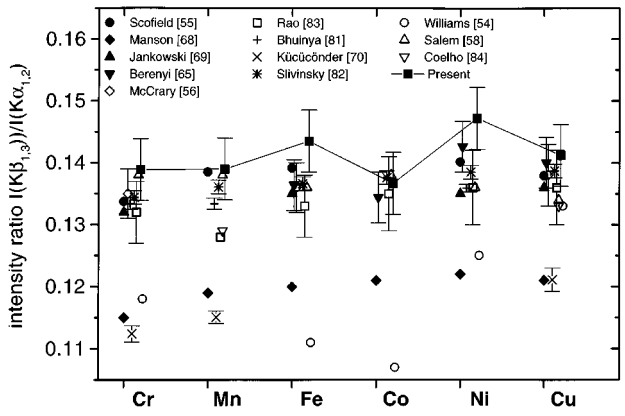

FIG. 5. The present, and previous, values of the $K\beta_{1,3}/K\alpha_{1,2}$ intensity ratio. Note the almost constant value across the range, and the strong underestimation by the theoretical values of Manson [68], and measurements of Kücükönder [70].

F. Fine structure of the $K\alpha$ doublet lines

Several studies reported observations of fine structure in the $K\alpha$ lines of the iron group elements. Schnopper and Kalata [71] reported such an observation for chromium, and further reports include chromium (Schnopper and Kalata [71], Shah and Das Gupta [72,73], and Priest [74]), iron (Priest [74]), cobalt (Shah and Das Gupta [73]), and copper (Sauder *et al.* [75]). By contrast, a large number of early and recently published studies failed to observe such structure [28,29,31,34,76–78]. In particular, no evidence for a fine structure was found in the high-resolution ($\Delta\lambda/\lambda = 9.7 \times 10^{-6}$) double crystal measurements of Onoue and Suzuki [44] for the chromium $K\alpha_1$ line, or the studies of Deutsch and co-workers [77,78] for Cu.

The resolution achievable in the single-crystal instrument used here is limited by the narrow but finite width of the spectrometer window. Using the values $\Delta\theta_s/\Delta\theta_d$ from Table I we roughly estimate that fine structure of width smaller than (0.05–0.12)×FWHM of the $K\alpha_1$ line, i.e., substructures with a FWHM smaller than 0.12–0.25 eV (depending on the different resolution settings for each measurement), cannot be resolved with our setup.

The accuracy of the present data is comparable with the results from two- and three-crystal spectrometers. The FWHM of the Cr $K\alpha_1$ peak, which was measured with the lowest-resolution setting of all of our measurements (see Table I) is 1.88 eV. It is found to be in excellent agreement with the 1.87-eV value of the high-resolution study of Onoue and Suzuki [44], measured using a double-crystal spectrometer with an asymmetric setup, and the 1.87 eV obtained in the triple crystal spectrometer measurements of Shah and

Das Gupta [73]. This agreement clearly demonstrates the good resolution and negligibly small instrumental broadening in our measurements. In spite of the good resolution no fine structure of the type reported in the studies mentioned above was detected in any of the spectral lines. While features of widths below our resolution, 0.1–0.25 eV, could hypothetically remain undetected, the existence of such features is highly unlikely considering the lifetime widths of the $3d$ transition metals' emission lines.

IV. CONCLUSIONS

We presented here results of a high-resolution and high-accuracy determination of the $K\alpha$ and $K\beta$ emission line shapes of the $3d$ transition metals chromium, manganese, iron, cobalt, nickel, and copper. The measurements were done using the same optimized single-crystal spectrometer, where special attention was given to minimizing the instrumental broadening effects. The lattice parameter of the perfect silicon crystal employed was determined on an absolute scale using combined x-ray and optical interferometry to a sub-ppm accuracy.

The most important results of this study are the determination of the absolute peak wavelengths of the lines on a metric scale to an accuracy of $\Delta\lambda/\lambda \sim 10^{-6}$ and the precise measurement of the emission line shape. This is imperative for the elucidation of the physical processes underlying the highly asymmetric x-ray lineshapes of the $3d$ transition metals. The linewidths and indices of asymmetry, determined from the measured spectra, compare well with the best previous measurements, and also with theoretical calculations taking into account the significant Coster-Kronig cross section. The curve of the $K\alpha$ widths vs Z shows a characteristic peak near the iron, while that of the $K\beta$ widths increases monotonically with Z. We also presented values for the $K\beta_{1,3}/K\alpha_{1,2}$ and $K\alpha_2/K\alpha_1$ intensity ratios. Both are somewhat higher than previous measurements though still within the combined experimental error of the best previous sets. Finally, an empirical fit by a minimal set of Lorentzians is presented for each spectrum, for use in accurate measurements requiring a correction for nonmonochromaticity, like structural refinements based on powder diffraction patterns.

The high-quality set of spectra obtained in this study provides a broad and accurate data base for testing theoretical calculations and predictions concerning the atomic structure and excitation and deexcitation dynamics in the $3d$ transition elements. In particular, it is hoped that a physically motivated study, now in progress, employing *ab initio* Dirac-Fock calculations and the present spectra will allow a definite resolution of the long standing question of the origin of the asymmetry of the x-ray emission lines of the $3d$ transition elements.

ACKNOWLEDGMENTS

Support by the Israel Science Foundation, Jerusalem, and the Bundesministerium für Forschung und Technologie under Contract No. 05 5SJAAI7 is gratefully acknowledged. We thank P. Becker (Physikalisch-Technische Bundesanstalt Braunschweig, Germany) for providing the calibrated silicon crystal used in the absolute wavelength measurements.

[1] M. Druyvesteyn, Z. Phys. **43**, 707 (1928).
[2] S. Doniach and M. Sunjic, J. Phys. C **3**, 285 (1970).
[3] K. Tsutsumi and H. Nakamori, in *X-Ray Spectra and Electronic Structure of Matter*, edited by A. Faessler and G. Wiech (Fotodruck Frank OHG, München, 1973).
[4] J. Finster, G. Leonhardt, and A. Meisel, J. Phys. (Paris), Colloq. **32**, C-4 (1971).
[5] M. Deutsch, G. Hölzer, J. Härtwig J. Wolf, M. Fritsch, and E. Förster, Phys. Rev. A **51**, 283 (1995).
[6] M. Deutsch, O. Gang, G. Hölzer, J. Härtwig, J. Wolf, M. Fritsch, and E. Förster, Phys. Rev. A **52**, 3661 (1995).
[7] M. Fritsch, C. C. Kao, O. Gang, and M. Deutsch (unpublished).
[8] J. Härtwig, G. Hölzer, J. Wolf, and E. Förster, J. Appl. Crystallogr. **26**, 539 (1993).
[9] H. Berger, X-Ray Spectrom. **15**, 241 (1986).
[10] J. Härtwig, G. Hölzer, E. Förster, K. Goetz, K. Wokulska, and J. Wolf, Phys. Status Solidi A **143**, 23 (1994).
[11] S. Grosswig, J. Härtwig, K.-H. Jäckel, R. Kittner, and W. Melle, Sci. Instrum. **1**, 29 (1986).
[12] (a) P. Becker, K. Dorenwendt, G. Ebeling, R. Laufer, W. Lucas, R. Probst, H.-J. Rademacher, G. Reim, P. Seyfried, and H. Siegert, Phys. Rev. Lett. **46**, 1540 (1981); (b) K. Nakayama and H. Fujimoto, IEEE Trans. Instrum. Meas. **46**, 580 (1997); (c) G. Basile, A. Bergamin, G. Cavagnero, G. Mana, E. Vittone, and G. Zossi, Phys. Rev. Lett. **72**, 3133 (1994).
[13] D. Windisch and P. Becker, Phys. Status Solidi A **118**, 379 (1990).
[14] B. Henke, E. Gullikson, and J. Davies, At. Data Nucl. Data Tables **54**, 181 (1993).
[15] W. Bond, Acta Crystallogr. **13**, 814 (1960).
[16] J. Härtwig, S. Grosswig, P. Becker, and D. Windisch, Phys. Status Solidi A **125**, 79 (1991).
[17] J. Wolf, Ph.D. thesis, Friedrich-Schiller-Universität Jena, 1994 (unpublished).
[18] E. Cohen and B. Taylor, Rev. Mod. Phys. **59**, 1121 (1987).
[19] J. Härtwig and S. Grosswig, Phys. Status Solidi A **115**, 369 (1989).
[20] B. Agarwal, *X-Ray Spectroscopy* (Springer-Verlag, Berlin, 1979).
[21] J. Thomsen, J. Phys. B **16**, 1171 (1983).
[22] W. Press, B. Flannery, S. Teukolsky, and W. Vetterling, *Numerical Recipes in PASCAL* (Cambridge University Press, Cambridge, 1989).
[23] *International Tables for X-Ray Crystallography*, edited by J.A. Ibers and W.C. Hamilton (Kynoch Press, Birmingham, 1974), Vol. IV. Note that the values in Vol. III as well as those in the new *International Tables of Crystallography*, edited by A.J.C. Wilson (Kluwer, Dordrecht, 1992), Vol. C, are taken from a compilation of Y. Cauchois and H. Hulubei, *Tables de Con-*

stantes et Donees Numeriques, I. Longueurs d'Ondes des Emissions X et des Discontinuites d'Absorption X (Hermann, Paris, 1947), which differ from the values employed here.
[24] R. D. Deslattes, Nucl. Instrum. Methods Phys. Res. B **31**, 51 (1988).
[25] J. Bearden, Rev. Mod. Phys. **39**, 78 (1967).
[26] R. Deslattes and A. Hennins, Phys. Rev. Lett. **31**, 435 (1973).
[27] R. Deslattes and E. Kessler Jr., IEEE Trans Instrum. Meas. **40**, 92 (1991).
[28] V. Pessa, E. Suoninen, and T. Valkonen, Phys. Fenn. **8**, 71 (1973).
[29] L. Parratt, Phys. Rev. **50**, 1 (1936).
[30] G. Brogren, Ark. Fys. **23**, 219 (1962).
[31] M. Blochin and I. Nikiforov, Bull. Acad. Sci. USSR **28**, 780 (1964).
[32] P. Lee and S. Salem, Phys. Rev. A **10**, 2027 (1974).
[33] A. Meisel and W. Nefedov, Z. Chem. **1**, 337 (1961).
[34] H. Sorum, J. Phys. F **17**, 417 (1987).
[35] I. Edamoto, Rep. Res. Inst. Tohoku Univ. A **2**, 561 (1950).
[36] U. Lehnert, K. Merla, and G. Zschornack, Nucl. Instrum. Methods Phys. Res. B **89**, 238 (1994)
[37] J. Bearden and C. Shaw, Phys. Rev. **48**, 18 (1935).
[38] J. Matthew, J. Nuttall, and T. Gallon, J. Phys. C **9**, 883 (1976).
[39] J. Fuggle and S. Alvarado, Phys. Rev. A **22**, 1615 (1980).
[40] K. Tsutsumi and H. Nakamori, J. Phys. Soc. Jpn. **25**, 1418 (1968).
[41] H. Sorum, O. Weng, and J. Bremer, Phys. Status Solidi B **109**, 335 (1982).
[42] H. Sorum, Phys. Status Solidi B **113**, 197 (1982).
[43] H. Sorum and J. Bremer, J. Phys. F **12**, 2721 (1982).
[44] K. Onoue and T. Suzuki, Jpn. J. Appl. Phys. **17**, 439 (1978).
[45] M. Krause and J. Oliver, J. Phys. Chem. Ref. Data **8**, 329 (1979).
[46] W. Nefedov, Bull. Acad. Sci. USSR **28**, 816 (1964).
[47] J. Fuggle, J. Electron Spectrosc. Relat. Phenom. **21**, 275 (1980).
[48] M. Hienonen, J. Leiro, and E. Suoninen, Philos. Mag. B **44**, 175 (1981).
[49] L. Yin, I. Adler, M. Chen, and B. Crasemann, Phys. Rev. A **7**, 897 (1973).
[50] R. Nyholm, N. Martenson, A. Lebulge, and U. Axelson, J. Phys. F **11**, 1727 (1981).
[51] D. M. Pease, Phys. Rev. B **44**, 6708 (1991).
[52] P. Chevallier, M. Tavernier, and J. Briand, J. Phys. B **11**, L171 (1978).
[53] R. Deslattes, R. LaVilla, P. Cowan, and A. Henins, Phys. Rev. A, **27**, 923 (1983).
[54] J. Williams, Phys. Rev. **44**, 146 (1933).
[55] J. Scofield, Phys. Rev. A **9**, 1041 (1974).
[56] J. H. McGrary, L. V. Singman, L. H. Ziegler, L. D. Looney, C. M. Edmonds, and C. E. Harris, Phys. Rev. A **4**, 1745 (1971).
[57] S. I. Salem and R. J. Wimmer, Phys. Rev. A **2**, 1121 (1970).
[58] S. I. Salem, T. Falconer, and R. Winchell, Phys. Rev. A **6**, 2147 (1972).
[59] Z. G. Pinsker, *Dynamical Scattering of X-Rays in Crystals* (Springer, Berlin, 1978).
[60] K. Heinrich, C. Fiori, and R. Myklebust, J. Appl. Phys. **50**, 5589 (1979).
[61] B. Dhal and H. Padhi, Phys. Rev. A **50**, 1096 (1994).
[62] J. Campbell, A. Perujo, W. Teesdale, and B. Millman, Phys. Rev. A **33**, 2410 (1986).
[63] G. Hölzer, computer codes DIXI and FITSPK (unpublished).
[64] D. Sewell, G. Love, and V. Scott, J. Phys. D **18**, 1233 (1985).
[65] D. Berényi, G. Hock, S. Ricz, B. Schlenk, and A. Valek, J. Phys. B **11**, 709 (1978).
[66] A. Perujo, J. Maxwell, W. Teesdale, and J. Campbell, J. Phys. B **20**, 4973 (1987).
[67] G. Paic and V. Pecar, Phys. Rev. A **14**, 2190 (1976).
[68] S. Manson and D. Kennedy, At. Data Nucl. Data Tables **14**, 111 (1974).
[69] K. Jankowski and M. Polasik, J. Phys. B **22**, 2369 (1989).
[70] A. Kücükönder, Y. Sahin, E. Büyükkasaps, and A. Kopya, J. Phys. B **26**, 101 (1993).
[71] H. Schnopper and K. Kalata, Appl. Phys. Lett. **15**, 134 (1969).
[72] M. Shah and K. Das Gupta, Phys. Lett. **29A**, 570 (1969).
[73] M. Shah and K. Das Gupta, J. Phys. Soc. Jpn. **37**, 1069 (1974).
[74] J. Priest, J. Appl. Phys. **42**, 4750 (1971).
[75] W. Sauder, J. Huddle, J. Wilson, and R. LaVilla, Phys. Lett. **63A**, 313 (1977).
[76] G. Brogren, Phys. Rev. **96**, 589 (1954).
[77] M. Deutsch and M. Hart, Phys. Rev. B **26**, 5558 (1982).
[78] N. Maskil and M. Deutsch, Phys. Rev. A **37**, 2947 (1988).
[79] A. Nigavekar and S. Bergwall, J. Phys. B **2**, 507 (1969).
[80] P. Sarode, X-Ray Spectrom. **22**, 138 (1993).
[81] C. Bhuinya and H. Padhi, J. Phys. B **25**, 5283 (1992).
[82] V. Slivinsky and P. Ebert, Phys. Rev. A **5**, 1581 (1972).
[83] N. Rao, S. Reddy, G. Satyanarayana, and D. Shastry, Physica C **138**, 215 (1986).
[84] L. Coelho, M. Gaspar, and J. Eichler, Phys. Rev. A **40**, 4093 (1989).
[85] E.R. Cohen, B.N. Taylor, CODATA Bull. No. 63 (1986).